Ultranarrow PbS Nanorod-Nematic Liquid Crystal Blend for Enhanced Electro-optic Properties

Sudarshan Kundu,[†] Jonathan P. Hill,[†] Gary J. Richards,[†] Katsuhiko Ariga,[†,§] Ali Hossain Khan,[||] Umamahesh Thupakula,[||] and Somobrata Acharya*[,||]

Liquid Crystal Institute, Tokyo University of Science-Yamaguchi, 1-1-1 Daigaku Dori, Onoda shi, Yamaguchi ken, 756 0884, Japan, World Premier International (WPI) Research Center for Materials Nanoarchitectonics (MANA), National Institute for Materials Science (NIMS), 1-1 Namiki, Tsukuba, Ibaraki, 305-0044, Japan, JST, CREST, 1-1 Namiki, Tsukuba, Ibaraki, 305-0044, Japan, and Centre for Advanced Materials (CAM), Indian Association for the Cultivation of Science, Jadavpur, Kolkata 700032, India

ABSTRACT Dispersion of ultranarrow PbS nanorods of 1.8 nm diameter, encapsulated by a fluidlike soft trioctylamine layer, in the nematic liquid crystal (LC ZLI-4792) results in a novel soft matter type blend with enhanced electro-optic properties. Despite having a cubic rock-salt structure, the ultranarrow rods possess a finite inherent dipole moment and show excellent miscibility in the LC host. The local ordering significantly affects the global ordering of the blend allowing a more rapid response of the electro-optic properties. These unique blends are obtainable only by doping with one-dimensional nanorods of ultrasmall dimensions and illustrates how a nonmesogenic element can be introduced within a liquid crystal for improvement of the switching properties of the blend. The unique blend could be a model for fundamental conceptual advances in general understanding of interaction behavior, leading consequently to a significant technological advancement for superior device fabrications.

KEYWORDS: ultranarrow PbS rods • nematic liquid crystal • blend • dipole moment • electro-optic properties

Liquid crystal display (LCD) devices are indispensable elements of modern life because of the ubiquity of their applications from wristwatch to personal computer displays. Control over the long-range orientational order of the LC is critical for obtaining superior optical switching and display device performance (1−8). However, control of long-range alignment of LCs has been remained challenging because of unaligned dislocation region formation, which is detrimental to LC device performance. The orientation of an LC is very sensitive to the topography, chemical nature, flow, or treatment of the cell surfaces (1, 7). Long-range alignment has been attempted by a variety of methods such as by use of alignment layers, by modification of the LC cells, or by utilizing the interaction between nanosized aggregates of LC molecules (7−11). Dispersions of nanomaterials in liquid crystals (LCs) as an active matrix component have attracted considerable scientific and technological attention in recent years, and that work has been motivated by demands for long-range alignment, manipulation of the LC orientation on a large scale and to fulfill the demand for faster switching speeds and higher contrasts of the devices (11−16). Additionally, the rapid development in synthesis control of nanocrystals has resulted in the emergence of an extensive class of inorganic materials with an impressive variety of sizes and shapes (17−20). However, for incorporation of the nanomaterials within an LC matrix, the proper selection of size, shape, and crystallographic phase of the nanomaterials is critical for boosting up the performance of the blend. Incorporation of nanomaterials into an LC matrix gives rise to the formation of topological defects due to deformations of the director field about the surface of the incorporated colloid species, which breaks the continuous symmetry of the blend (6, 11, 13−15). Topological defects become more serious with impregnation of materials of larger dimensions and use of higher concentrations. To gain an understanding of such defects caused by dopant particles in a complex fluid and to exert control over the defects are significant scientific challenges.

The shape and crystallographic phase of the nanomaterials are also important when considering the long-range ordering of the blend. For example, zero-dimensional (0D) spherical nanomaterials lack anisotropy and inappropriate for long-range-ordered structures. On the other hand, one-dimensional (1D) nanomaterials possessing an inherent dipole moment respond in an external field facilitating alignment along the direction of the field (21, 22). Because LCs are also sensitive to an external field, blends consisting of 1D nanomaterials and LC may demonstrate singular behavior under application of an external field upon proper dispersion. Thus, anisotropic nanomaterials of proper dimensions coupled locally with the director field in a favor-

* Corresponding author. E-mail: camsa2@iacs.res.in.
Received for review March 30, 2010 and accepted September 21, 2010
[†] Tokyo University of Science-Yamaguchi.
[‡] National Institute for Materials Science.
[§] CREST.
[||] Indian Association for the Cultivation of Science.
DOI: 10.1021/am100599y

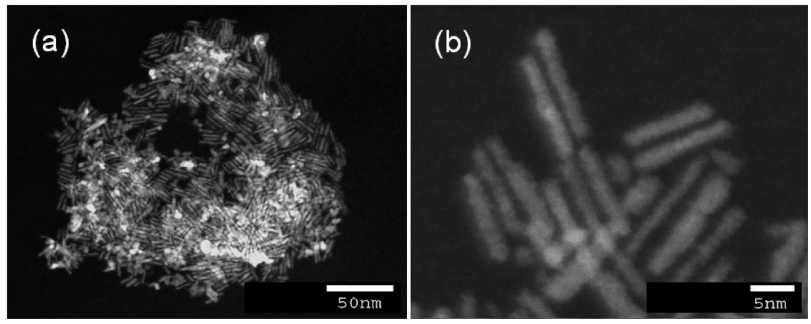

FIGURE 1. (a, b) Dark-field TEM images of ultranarrow PbS rods at different magnifications. The diameter of the nanorods is 1.8 ± 0.2 nm, whereas the length of the nanorods is 12−15 nm.

able energetic configuration might enhance long-range ordering and LC device performance. PbS, with large exciton Bohr radius (20 nm), is extremely important for fundamental confinement dependent studies and technological development is specially promising for a large number of applications in the mid- and near- infrared devices. Here we show that dispersion of ultranarrow atomic scale PbS rods encapsulated by a fluidlike soft organic layer of trioctylamine (TOA) dispersed in the nematic LC ZLI-4792 results in a soft matter type blend with enhanced application properties. These ultrasmall nanorods possess dipole moment and show excellent miscibility in the LC host even at high concentrations. The local ordering significantly affects the global ordering of the blend in response to the external electric field allowing the electro-optic properties to be tailored. The incorporation of atomic scale 1D PbS rods in complex LC ZLI-4792 makes the blend attractive as a model system for studying the interaction behavior in a controllable way and to explore their potential for superior device applications.

We have recently reported on ultra narrow nanorods and nanowires of type II−IV materials by decomposition of single precursor metal xanthate in suitable ligand using a single-step synthesis route (21−23). The decomposition of single molecule precursor usually result in highly crystalline nanomaterials of narrow size distribution with a high degree of shape control (16−18, 21−23). The key of successful size and shape control generally depends on the proper choice of precursor, reagent concentrations and reaction temperature. However, the preparative approach of metal xanthate is different in each case and depends on the type of metal salt used. The synthetic approach of size-controlled ultra narrow PbS rods is based on the decomposition of single precursor lead-hexadecylxanthate in a single step in trioctylamine (TOA) as surfactant cum solvent at low temperature at 80 °C (see experimental details) (24). Images a and b in Figure 1 show the dark-field (DF) transmission electron microscopy (TEM) images of TOA-coated PbS rods of 12−15 nm in length. No additional postsynthesis stages were adopted for the size selectivity of these ultranarrow rods. The ultra narrow rods are highly monodispersed as depicted in the large-area TEM image (Figure 1a).

The bright-field high-resolution TEM (HRTEM) images of individual rods show that the inorganic cores are of 1.8 ± 0.2 nm in diameter (Figure 2a) with well-resolved lattice planes corresponding to interplanar distance of 0.29 ± 0.02 nm, consistent with the (200) *d*-spacing of PbS bulk rock-salt structure. The interplanar distance 0.42 ± 0.02 nm observed in HRTEM corresponds to the (220) sets of planes of PbS rock-salt structure. The HRTEM image indicates an orientation in which the ⟨110⟩ crystallographic axis is parallel to the long axis of the rods. Energy-dispersive X-ray analysis (EDS) carried out in TEM reveals a Pb to S ratio of ∼1:1, as expected for a stoichiometric crystal (Figure 2b).

The selected area electron diffraction (SAED) patterns of these ultranarrow PbS rods (Figure 2b, inset) shows the rock salt cubic structure with predominant 200 and 220 diffraction rings, corresponding to the interplanar distances of 0.2969 and 0.2099 nm of PbS bulk rock salt structure (JCPDS powder diffraction file #05−0592). The strongest intensity of the 200 reflection is in-line with the expected 200/220 intensity ratio of 1:0.57 in the JCPDS powder diffraction file. We have analyzed the growth directions using DM3 software provided by JEOL. The software allows generating Fast Fourier Transformation (FFT) from a selected frame of the HRTEM image. Figure 2c shows the FFT generated from the HRTEM image shown in Figure 2a. The FFT clearly shows two sets of spots which respectively correspond to the (200) planes and (220) planes. A profile analysis using DM3 software permits an accurate determination of the lattice spacings. The inverse FFT regenerates the HRTEM image with much higher resolution, from which the statistical profile analysis can be made again to tally the *d*-spacings. The profile analysis of lattice spacings (figure 2d and 2e) confirms the interplanar distance of 0.42 nm corresponding to (220) and interplanar distance of 0.29 nm corresponding to (200) *d*-spacing of PbS bulk rock salt structure. The difference of *d*-spacings between (200) and (220) planes are within the resolution of HRTEM and are therefore confirmed using fast Fourier transform.

The initial PbS seed is presumably terminated by {100}, {110}, {111} or their equivalent facets. High-index planes generally exhibit much higher activity, because they have a high density of atomic steps, which usually serve as active sites for breaking of chemical bonds. Out of these facets, {110} and {100} or their equivalent facets consist of mixed atoms and {111} facets consist of either Pb or S atoms (Figure 3b−d). Because of the mixed nature of {100} and {110} facets, the ligand adsorption kinetics differ from those

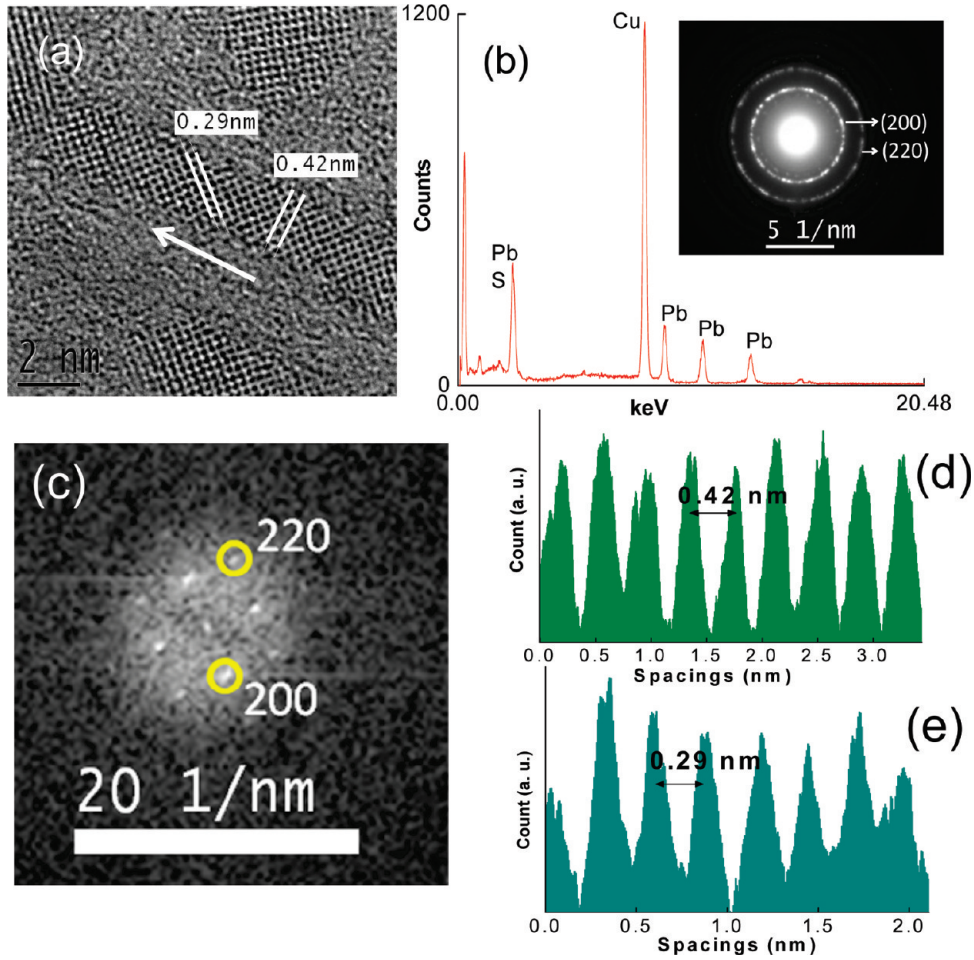

FIGURE 2. (a) HRTEM image of ultra narrow PbS rods showing diameter of 1.8 nm with well-resolved lattice planes. The interplanar distance of 0.42 ± 0.02 nm corresponds to the (220) sets of *d*-spacings along which the growth occurs for the long axis of the nanorod. The arrow indicates the growth direction of the PbS rods. (b) Energy-dispersive spectroscopy (EDS) elemental analysis spectra taken in the TEM of PbS 1.8 nm diameter rods. The EDS reveals a nearly stoichiometric ratio of Pb to S. Inset, SAED pattern from the ultranarrow rods. (c) FFT of PbS rod taken from part of the HRTEM image. Profile analysis of lattice spacing of (d) PbS (220) planes and (e) PbS (200) planes.

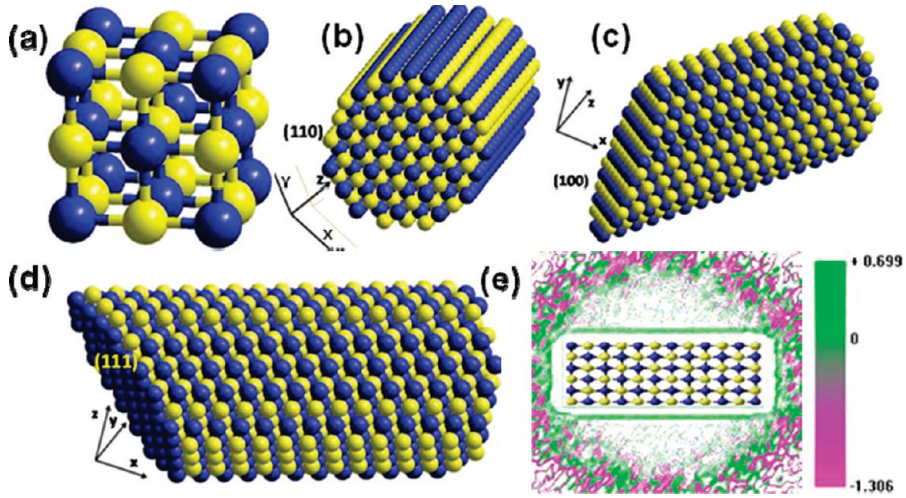

FIGURE 3. (a) Ball-and -stick model of cubic rocksalt PbS structure (blue and yellow represents lead and sulfur atoms, respectively. (b−d) Lower and higher indexed facets (110), (100), and (111), respectively, of PbS rock-salt structure. (e) Simulated contour map of potential distribution of the rod having 3 × 3 × 6 unit cells using Molecular Mechanics algorithm with green representing positive potential and red representing the negative potential.

at the {111} facets. The use of amines as capping ligand plays an important role in determining the nanocrystal shape and size in addition to stabilizing the particles (21−23, 25, 26). The alkyl amines are Lewis bases; the long alkyl chains length provide an increased electron density on the nitrogen site thus inducing metal coordination. Note the

reduced size of the rods imply an increased surface to volume ratio which increases the number surface atoms. Because the surface atoms consist of both lead and sulfur atoms, there are a large number of lead atoms on the surface of PbS rods for coordination with the ligand trioctylamine. The presence of a large number of metal atoms on the surface in nanorods will allow better passivation with the ligands for PbS rods. It is expected that because of its greater nucleophilicity, TOA should bind to the lead ions of the inorganic core of the nanorods, at least as strongly as in the case of previously used primary amine capping agents (21−23). Stabilizing alkyl amines adsorb well only at planes rich in metal ions leaving the other chalcogenide sites free. The growth rate and kinetics of ligand adsorption differ markedly at the different initially available PbS rock salt facets, which is crucial for developing these ultranarrow rods (27). Because the {111} facets are terminated either by Pb or by S atoms, the ligand binds strongly to the metal atoms facilitating asymmetric growth. Under faster growth at elevated temperature, elimination of {111} facets occurs. Compared to {110} facets, {100} facets have a higher kinetic energy barrier, while the {110} facets have higher surface energy [E(surface) = n (hkl)], facilitating growth along the ⟨110⟩ direction.

Although a large dipole moment may be expected for wurtzite nanocrystals due to existence of noncentrosymmetric alternate stacking (28), it ought to be absent in cubic nanocrystals with center of symmetry (Figure 3a). However, centrosymmetric nanocrystals may exhibit size-dependent dipole moments depending on the arrangements of atoms on different facets (29, 30). The lower indexed facets are mixed in nature, however, the difference in electronegativity between Pb and S may result in weak polarity in some of these mixed facets (Figure 3b,c). However, the major contribution comes from the high index facets, which are formed either by Pb or S (Figure 3d). Because of the difference in electronegativities between Pb and S, high index facets are polar and their arrangement defines the overall electronic charge distribution within the PbS nanorod (30). The HRTEM investigations of PbS nanorods evolves different growth directions (Figure 2a) of rock salt crystal structure (Figure 3a). The HRTEM image indicates an orientation in which the ⟨110⟩ crystallographic axis is along the long axis of the rods and the interplanar distance 0.29 ± 0.02 nm observed in HRTEM corresponds to the (200) plane of PbS rock salt structure. The reconstruction of HRTEM images revealed that the PbS nanorods are terminated by four {100} facets at the surface and two {110} facets at the ends of the nanorods. Both the {100} and {110} facets are consisting of mixed atoms. The reconstructed image (Figure 3d) also reveals four higher indexed {111} facets either consists of Pb or S atoms. Because of the difference in electronegativities between Pb and S, {111} facets are polar and their spatial arrangement will determine the overall electronic charge distribution and dipole moment within the PbS rods (30).

Additionally, a deviation in the shape from centrosymmetry could induce a dipole moment that depends on the size and volume of the nanocrystal (30). The facile formation of rods along ⟨110⟩ direction results in the essential chemical and electrostatic anisotropy of the rods (Figure 3e). We can estimate a 1.24D dipole moment per rod using the relation, $\mu = 1.27(3\varepsilon_S/(2\varepsilon_S + \varepsilon))V$, where V is the volume of the nanorod and ε_S, ε are the dielectric constants of the surrounding matrix (i.e., trioctylamine surfactant layer around PbS rods) and core PbS, respectively (31, 32).

We used a fluorinated nematic liquid crystal blend ZLI-4792 with clearing temperature 92 °C and refractive index 1.49 as host matrix keeping in mind the compatibility of refractive index of the LC with that of TOA (1.448), and with lower ionic impurity content compared to other commonly used testing liquid crystals like the cyanobiphenyl derivatives (5CB, 8CB). A component is miscible to other when there is a matching of dielectric constant or refractive index. The dielectric constant of a solvent is a relative measure of its polarity and solubility, consequently the matched refractive index of ZLI-4792 and TOA certainly points out about the miscibility of two components. The ultranarrow PbS rods were used as dopant at different volume ratios in the ZLI-4792 host matrix. Using refractive index matched surfactant coated nanorods as the dopant offers additional advantages in the present case. First, the surfactant amine layer allows the inorganic core to maintain its inherent physical properties and robustness, whereas the inorganic core itself does not come into direct contact with the liquid crystal since only the soft and fluid like organic-coated surface is exposed. Second, the nanorods are readily miscible in the liquid crystal host matrix because of the close match in refractive index and to the inter-rod van der Waals screening forces due to the presence of the surfactant coating (32, 33).

Nematic liquid crystals are composed of rodlike molecules with the long axes of neighboring molecules mutually approximately aligned. To allow this anisotropic structure and represent the local average orientation, we introduced a dimensionless unit vector called the director to represent the direction of preferred orientation of molecules in the neighborhood of any point. One of the important features of the nanorods' interaction with the liquid crystalline host is their anchoring behavior at the interface. When anisotropic nanorods with large dipole moment are added to the polar liquid crystalline host, the large dipole−dipole interaction between the dopant and host might lead to the aggregation of the nanorods. The aggregation of the nanorods will in turn induce dislocations, which is detrimental for long-range alignment and faster switching speed. The existence of a weak dipole moment in PbS nanorods do not promote strong coupling with the LC matrix, rather they stay as individual entities within the host ZLI-4792 matrix because of lower dipole−dipole interaction and inter-rod van der Waals screening forces by the surfactant coating.

Thus, in the equilibrium condition, the PbS nanorods should "float" inside the liquid crystals, under which different types of boundary conditions on the rod surface may exist. When the nanorods are dispersed within the host LC, the director field in the vicinity of the nanorods will be distorted, whereas the orientation will remain fixed far from the nanorod site. Because the director field is influenced by the rods near the surface, this should influence the orientational order of the nanorods to generate energetically preferred orientations at the expense of nematic elastic energy (14). Eventually, the nanorods can anchor locally in a number of ways with the director (16). Possible anchoring conditions may be in three mutually orthogonal configurations, namely: (i) with director parallel to the main axis of the nanorod (ii) with director perpendicular to the rod axis and tangential to its lateral surface and (iii) with director perpendicular to the particle surface. The director field distorts at the interface to satisfy interfacial boundary conditions, generating a restoring torque that attempts to reorient the nanorods in an equilibrium position of lowest possible energy. The free energy of the blend consisting of PbS rods and ZLI host, which is the lowest energy orientational state of the nanorods for different types of anchoring conditions, reveal the equilibrium upon minimization. In the case of these blends, the expression for free energy should be the sum of both volume and surface contributions of the orientational elastic origin produced in the presence of nanorods integrated over the LC specimen volume surrounding the rod surface and particle surface, respectively. In principle, the Frank elastic coefficients are case dependent. However, the isotropic condition [K (elastic constant) = K_{11} (for splay) = K_{22} (for twist) = K_{33} (for bend)] can be used for simplicity reducing the number of elastic coefficients to one (35). In simplified form, the free energy of this mixed component (14, 34−36) is the sum of the anchoring energy at the rod surface and the elastic energy of the LC volume surrounding the rod surface

$$F = K\int_S d^3r\frac{1}{2}\sum[P_i n(r_\alpha)]^2 + K\int_V d^3r\frac{1}{2}\sum(\nabla_i n_j)(\nabla_i n_j)$$

In the above equation, $n(r)$ is the Frank director that specifies the direction of local alignment of anisotropic LC molecules at the point r (x, y, z). Notably, nematic LCs are invariant under the inversion operation $n(r) = -n(r)$. The first term of the above equation represents the interaction between the nanorods and the director that may lead to long-range alignment. Since the individual nanorod consists of dipole moment (p), there will be a dipole-moment density for a collection of nanorods at positions r_α given by $P_i = \Sigma p_i$. This term basically represents the energetic preference for the nanorods to align either parallel or antiparallel to the director. The integral is over the volume of the nematic LC; $i,j = x, y, z$; n_i is the ith component of the director, and $\nabla_i = \partial/\partial x_i$. Upon minimization, the free energy leads to an equilibrium orientational positioning of the nanorods with the nematic director depending on the anchoring conditions.

In the extremum equilibrium position, the rods will either be parallel or perpendicular to the nematic director depending upon the unitless anchoring strength ratio $\omega = WR/K$, where W is the surface energy, R is the rod radius, and K is the Frank elastic constant in one constant approximation (35). The parameter ω determines the degree of anchoring for a given pair of nanorod and LC blend. Depending upon the strength of ω, the equilibrium position of the nanorod may be either parallel ($\omega < 1$) or perpendicular ($\omega > 1$) to the director of a liquid crystalline domain. Our estimation using the realistic physical parameters $R = 0.9 \times 10^{-9}$m, $K = 13 \times 10^{-12}$ N, $W = 3.92 \times 10^{-5}$ J m^{-2} underestimates the strong anchoring with $\omega < 1$, which is in line with the weak dipole moment of the nanorods. On the other hand, in a longitudinal anchoring approximation where the long axes of the nanorods are parallel with the nematic director (the first case as discussed above), the energy (F_L) varies quadratically with the nanorod orientations as $F_L = 2\pi KC\theta^2$, where $C \approx L/2\ln A$ is the capacitance of a rod of length L with aspect ratio A (14, 34). Thus, longitudinal anchoring seems to be a reasonable choice for the coalignment as the probable equilibrium position irrespective of the boundary conditions. As a consequence of the rods' ultrasmall dimensions, less torque is required to reorient the rods in the energetically favored longitudinal configuration. The preferred longitudinal anchoring of the nanorods within the liquid crystalline blend has important implications for the long-range alignment and on the optical polarization behavior of the blend. When an electric field is applied, the blend aligns along the direction of the field producing a global unidirectional orientation of the rods and LC directors, and defining a unique axis for the system.

The voltage at which the LC molecules start rotating is called threshold voltage (V_{th}), which defines the minimum voltage required for a specific LC cell to work. The preferred longitudinal anchoring of the nanorods with the LC director stimulates an electro-optic response by lowering the V_{th} of the blend. The voltage versus transmission curve (Figure 4a) demonstrates that V_{th} of the blend was substantially reduced by up to 5% compared to pristine ZLI-4792. The lowering of V_{th} is caused by the effective dielectric anisotropy ($\varepsilon_{rod,\ LC} > \varepsilon_{LC}$) of the composite system, which results in a larger torque for the blend ($\varepsilon_{rod,\ LC}E^2 > \varepsilon_{LC}E^2$) in an applied field, causing faster alignment. The contrast ratio is the ratio of the maximum luminosity to dark at the center of the panel, which is a measure of quality of a display system. By definition, contrast ratio is unitless and physically defines the percentage of the transmission of light through a LC cell. A high contrast ratio is desired for a quality display and sharpness of the picture on a LCD screen. Improvement of the contrast ratio in LCD displays has been a major topic of research. Unlike active element electronic displays (CRT, electroluminescent and LED displays, OLED, etc.), the LCD matrix is a passive emitter. LCD cannot generate light; rather, it modulates the light passing through it. The LCD controls opacity in the presence of an external voltage thus defining the contrast ratio. Thus, a LCD cell works as an

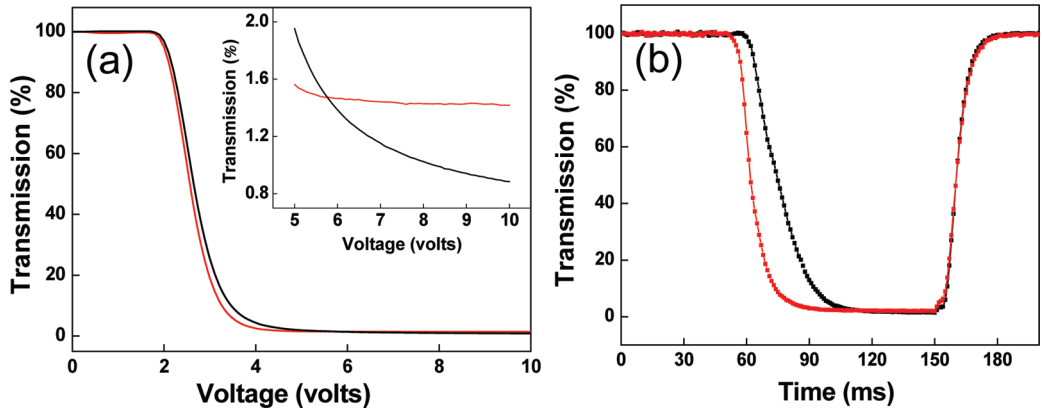

FIGURE 4. Electro-optic response from 5 μm thick cells of ZLI-4792 (black curve) and PbS nanorod blended cells at 20% volume ratio (red curve): (a) Voltage versus transmission curve demonstrating a lowering of threshold voltage upon nanorod mixing. Inset, expansion of higher voltage region. (b) Transmission versus time optical response for applied voltage (5 V) of ZLI-4792 and PbS nanorod blends placed between crossed polarizers. Both transmission states correspond to two stable orientational states of the blend with field on and off conditions.

optical shutter, which basically controls the light throughput through a LC cell.

To measure contrast ratio, we measured the light throughput across a LC prototype cell with a change in applied voltage. Normally, a signal of a few kilohertz with square wave voltage is applied to the cell. The scale is made in such a way that the light throughput at 0 V is set to 100, which is the convention to measure static contrast ratio in a TN LCD. As the applied voltages increases, the liquid crystal molecules start rotating along the direction of the electric field. After crossing, as the applied voltage increases, the light throughput drops sharply; at a higher value of applied voltage, the light throughput saturates at a lower value. The ratio of light throughput at 0 V and the light throughput at higher voltage where the transmission data saturates near "zero" defines the contrast ratio.

The voltage versus transmission curve (inset of Figure 4a) demonstrates that the conventional static contrast ratio of the blend has been reduced compared to the pristine ZLI-4792 at 10 V. However, the implementation is significant while considering the gray scale switching. In forming a picture using LCD display, the switching speed for bright-gray-bright transition is important in addition to bright-dark-bright state. In the case of a bright-dark-bright transition, LC molecules have to rotate more in comparison to bright-gray-bright transitions, which requires a longer switching time. In order to achieve 50% transmission (a gray state of pixel), which is needed for a monochrome display panel, a higher field is required to change the orientation of the pure LC molecules. Hence it is important to improve the switching speed for the gray scale. Although the contrast ratio of LC-PbS blend has been degraded in the conventional sense, a faster gray scale switching can be achieved with ease.

The response time defines how fast a device can switch from a state of 90% light throughput (on state) to a state of 10% light throughput (off state) or vice versa. The field "on−off" electro-optical responses with nanorods-doped blend demonstrate the faster response times compared to neat ZLI-4792 (Figure 4b). The switching time for the on-state in nanorod LC blend is 16 ms, whereas the same for the LC is 28 ms with both data taken at 5 V. Switching off the field results in a rapid increase in transmission with a profile almost complementary to that for the field-on conditions indicating a rapid return to the initial disordered state of the ZLI-4792-nanorod blend (Figure 4b). Thus, on−off states reveal a faster switching speed for the PbS-LC blend in comparison to the pristine LC. Notably, the relaxation time calculated for a single rod results in a field-off time of the order of milliseconds. The relaxation time ~3 ms obtained from $\Gamma r = (3/\pi D_R)(\ln 2l/d - 0.8)$ for the nanorods upon removal of the field matches reasonably with the observed field-off response time (28, 35). Note that its always not required to reach the darkest state to form a picture in a display, however, its also important to see the switching speed of a bright-gray-bright transition (gray scale switching) instead of bright-dark-bright state. To observe the gray scale switching, the on-time and off-time at 5 V is important. The traditional measure of response time of a TNLCD is the total time taken for a pixel to change its state from bright to dark and back to bright state again. More precisely, it is the time for the pixel's brightness to drop from 90 to 10% and then grow to 90% again. For white to gray switching, instead of white to black, the blend has to orient to a smaller degree, but the speed of orientational change should be proportional to the magnitude of the applied field. Now to get a 50% transmission (a gray state of pixel) with pure LC system, which is needed for a monochrome display panel, higher field is required to change the orientation of the pure LC molecules. With incorporation of PbS nanorods in LC, one can get 50% transmission (the gray state of pixel) faster and can return back to the 100% transmission state as quickly as pure LC. Our measurement suggests bright to dark state switching at 5 V operating voltage while the dark-bright-dark switching time remains the same for both pure ZLI-4792 and nanorod blend, which suggests an improvement in gray scale switching speed with the nanorod blend. The improvement in threshold voltage and faster response time are crucial from the point of view of applications of LC devices.

In conclusion, we have reported on a novel blend comprising of ultranarrow PbS nanorods and a nematic liquid

crystal (LC ZLI-4792). The dispersion of ultranarrow PbS rods encapsulated in a fluid-like soft organic layer of trioctylamine (TOA) in a nematic liquid crystal (LC ZLI-4792) results in a soft matter type blend with excellent miscibility in the LC host. The incorporation of 1D nanorods enhances the electro-optic performance of the blended cells. However, selection of nanomaterial dopant species is not limited to the anisotropic nanorods. Rather, those with strong inherent dipole moments, of low dimensionality comparable to the host LC molecules, of narrow size distributions, or possessing a suitable surfactant coating with refractive index closely matching that of the host LC are the important choices. Combinations of nanomaterials with liquid crystals might also meet subcomponent manufacturing standards and offer fabrication possibilities for devices with improved contrast ratios and faster switching speeds.

EXPERIMENTAL METHODS

Synthesis. For the synthesis of 1.8 nm diameter rods, lead hexadecylxanthate (0.065 g) was added in one portion to 1.6 mL of trioctylamine (Aldrich, 98%) at 65 °C with continuous stirring under N_2. A milky-grayish color appeared after 5 min. The temperature was then increased to 80 °C and annealing was carried for 40 min at this temperature. The temperature was reduced to 50 °C and the rods were collected by washing by centrifuging twice with methanol then finally with a mixture of dichloromethane and methanol (5:40 by volume) to remove excess surfactants. For each wash, the centrifuge was rotating at speed of 3000 rpm for 3 min. The nanorods were dried and redispersed in toluene to prepare a standard stock suspension of concentration 1.0 mg/mL.

HRTEM. High-resolution transmission electron microscopy (HRTEM) was performed by using a JEOL-JEM2000 operating at 200 kV. Samples were cast onto carbon-coated copper grids and dried in vacuo prior to observations.

Liquid Crystal Device Preparation. Different volumes of PbS nanorods from standard stock suspension were blended with a fixed volume of ZLI-4792 (100 μL, 0.268 g). The best performance of the LC cells was obtained by blending 20 μL of PbS suspension in 100 μL ZLI-4792. Data presented here were obtained using such a sample. LC cells, consisting of two indium tin oxide (ITO)-coated glass substrates as counterelectrodes, were fabricated according to a standard procedure in a clean room environment. The separation distance between the ITO plates was fixed at 5 μm using a silica bead spacer. SE130 was used as an aligning agent. Cells were filled with pure LC (ZLI-4792) and nanorod-LC blend by capillary action. An Otsuka Electronics Co. Ltd. LCD 5200 was used to measure the voltage versus transmission performance and the response time dependence. The LCD5200 is an instrument used in the LCD industries to characterize liquid crystal display devices through measurements of optical throughput, contrast ratio, switching time, viewing angles, etc. The instrument consists of an airtight chamber, inside which there is a visible light source, two polarizers (one polarizer and one analyzer) and an optical sensor. The LCD prototype is placed in between the polarizer and the analyzer and the cell is irradiated with white light in the visible range. The position of LCD prototype is adjusted so that maximum light throughput can be achieved. A 50 Hz square voltage is applied, which is the driving voltage for an LCD device, and optical transmission is measured using an optical sensor placed behind the analyzer.

Computational Details. To determine the potential distribution in the cubic PbS nanorod, we generated a 3 × 3 × 6 unit-cell-sized model and applied a finite electric field of 0.00001 a. u. along the *z*-direction in a vacuum. The PbS nanorod is also aligned along the direction of the electric field. In MM+, we have set the electrostatic contribution from the atoms as bond dipole moments associated with polar bonds instead of setting atomic charges for atoms. In order to consider the extent of interaction of these atomic dipoles with the surrounding dipoles, a smoothing function called "switched" was applied from the inner radius to the outer radius, with in this limit the nonbonded interactions reduce gradually to zero. The inner radius defines the maximum interatomic distance for full nonbonded interactions and outer radius defines the minimum distance at which nonbonded interactions are set to zero. The structure was minimized using a single point minimization. After obtaining the minimum energy configuration of the lattice, 2D contour maps of potential distribution across PbS nanorod could be obtained with the *z*-direction as reference direction.

Acknowledgment. Financial support from Centre for Nanotechnology for Photovoltaics and Sensor Devices, DST, Government of India, Grant SR/S5/NM-47/2005, Grant SR/NM/NS-49/2009, and World Premier International Research Center Initiative (WPI Initiative) on Materials Nanoarchitectonics, MEXT, Japan, and Core Research for Evolutional Science and Technology (CREST) program of Japan Science and Technology Agency (JST), Japan, are gratefully acknowledged.

REFERENCES AND NOTES

(1) de Gennes, P. G. *The Physics of Liquid Crystals*; Clarendon Press, Oxford, U.K., 1974.
(2) Robbie, K.; Broer, D. J.; Brett, M. J. *Nature* **1999**, *399*, 764–765.
(3) Grollau, S.; Abbott, N. L.; de Pablo, J. J. *Phys. Rev. E* **2003**, *67*, 051703−0517012.
(4) Fukuda, J.; Yoneya, M.; Yokoyama, H. *Phys. Rev. E* **2002**, *65*, 041709−041713.
(5) Loudet, C.-J.; Barois, P.; Poulin, P. *Nature* **2000**, *407*, 611–612.
(6) Andrienko, D.; Allen, M. P.; Skacej, G.; Zumer, S. *Phys. Rev. E* **2002**, *65*, 041702−041709.
(7) Woltmann, S. J.; Jay, G. D.; Crawford, G. P. *Nat. Mater.* **2007**, *6*, 929–938.
(8) Ariga, K.; Hill, J. P.; Lee, M. V.; Vinu, A.; Charvet, R.; Acharya, S. *Sci. Technol. Adv. Mater.* **2008**, *9*, 014109−014205.
(9) Luk, Y.; Abbott, N. L. *Science* **2003**, *301*, 623–626.
(10) Yamamoto, J.; Tanaka, H. *Nature* **2001**, *409*, 321–324.
(11) Yada, M.; Yamamoto, J.; Yokoyama, H. *Phys. Rev. Lett.* **2004**, *92*, 185501–185505.
(12) Williams, Y.; Chan, K.; Park, J. H.; Khoo, I. C.; Lewis, B.; Mallouk, T. E. *Proc. SPIE* **2005**, *5936*, 593613–593619.
(13) Wu, K.-J.; Chu, K.-C.; Chao, C.-Y.; Chen, Y.-F. *Nano Lett.* **2007**, *7*, 1908–1913.
(14) Lapointe, C.; Hultgen, A.; Silevitch, D. M.; Felton, E. J.; Reich, D. H.; Leheny, R. L. *Science* **2004**, *303*, 652–655.
(15) Koenig Jr, G. M.; Meli, M.-V.; Park, J.-S.; de Pablo, J. J.; Abbott, N. L. *Chem. Mater.* **2003**, *19*, 1053–1061.
(16) Acharya, S.; Kundu, S.; Hill, J. P.; Richards, G. J.; Ariga, K. *Adv. Mater.* **2009**, *21*, 989–993.
(17) Acharya, S.; Sarma, D. D.; Golan, Y.; Sengupta, S.; Ariga, K. *J. Am. Chem. Soc.* **2009**, *131*, 11282–11283.
(18) Pradhan, N.; Acharya, S.; Ariga, K.; Karan, N. S.; Sarma, D. D.; Wada, Y.; Efrima, S.; Golan, Y. *J. Am. Chem. Soc.* **2010**, *132*, 1212–1213.
(19) Lu, J. G.; Ye, Z. Z.; Zhang, Y. Z.; Liang, Q. L.; Fujita, S.; Wang, Z. L. *Appl. Phys. Lett.* **2006**, *89*, 023122−023125.
(20) Tang, Z.; Kotov, N. A.; Giersig, M. *Science* **2002**, *297*, 237–240.
(21) Acharya, S.; Panda, A. B.; Efrima, S.; Golan, Y. *Adv. Mater.* **2007**, *19*, 1105–1108.
(22) Acharya, S.; Patla, I.; Kost, J.; Efrima, S.; Golan, Y. *J. Am. Chem. Soc.* **2006**, *128*, 9294–9295.
(23) Panda, A. B.; Acharya, S.; Efrima, S. *Adv. Mater.* **2005**, *17*, 2471–2474.
(24) Acharya, S.; Gautam, U. K.; Sasaki, T.; Bando, Y.; Golan, Y.; Ariga, K. *J. Am. Chem. Soc.* **2008**, *130*, 4594–4595.
(25) Patla, I.; Acharya, S.; Zeiri, L.; Israelachvili, J.; Efrima, S.; Golan, Y. *Nano Lett.* **2007**, *7*, 1459–1462.

(26) Yuhas, B. D.; Zitoun, D. O.; Pauzauskie, P. J.; He, R.; Yang, P. *Angew. Chem., Int. Ed.* **2006**, *45*, 420–423.
(27) Lee, S.-M.; Cho, S.-N.; Cheon, J. *Adv. Mater.* **2003**, *15*, 441–444.
(28) Li, L. S.; Alivisatos, A. P. *Phy. Rev. Lett.* **2003**, *90*, 097402–097406.
(29) Shim, M.; Guyot-Sionnest., P. *J. Chem. Phys.* **1999**, *111*, 6955–10.
(30) Cho, K. S.; Talapin, D. V.; Gaschler, W.; Murray, C. B. *J. Am. Chem. Soc.* **2005**, *127*, 7140–7147.
(31) Nann, T.; Schneider, J. *Chem. Phys. Lett.* **2004**, *384*, 150–152.
(32) Min, Y.; Akbulut, M.; Belman, N.; Golan, Y.; Zasadzinski, J.; Israelachvili, J. *Nano Lett.* **2008**, *8*, 246–252.
(33) Kane, R. S.; Cohen, R. E.; Silbey., R. *J. Phys. Chem.* **1996**, *100*, 7928–7932.
(34) Brochard, F.; de Gennes., P. G. *J. Phys. (Paris)* **1970**, *31*, 691–708.
(35) Burylov, S. V.; Raikher, Y. L. *Phys. Rev. E* **1994**, *50*, 358–367.
(36) Lynch, M. D.; Patrick., D. L. *Nano Lett.* **2002**, *2*, 1197–1201.

AM100599Y